Growth of nanometer thin ice films from water vapor studied using scanning polarization force microscopy

Hendrik Bluhm and Miquel Salmeron

Citation: The Journal of Chemical Physics **111**, 6947 (1999); doi: 10.1063/1.479987
View online: http://dx.doi.org/10.1063/1.479987
View Table of Contents: http://scitation.aip.org/content/aip/journal/jcp/111/15?ver=pdfcov
Published by the AIP Publishing

Growth of nanometer thin ice films from water vapor studied using scanning polarization force microscopy

Hendrik Bluhm and Miquel Salmeron[a)]
Materials Sciences Division, Lawrence Berkeley National Laboratory, University of California, Berkeley, California 94720

(Received 29 January 1999; accepted 21 July 1999)

Atomic force microscopy (AFM) was used to study the growth and morphology of ice films on the cleavage surface of mica. Measurements performed in contact, as well as in noncontact operation modes of the microscope, allowed us to distinguish the solid and liquid parts of the film. At temperatures below −30 °C, supercooled water droplets formed on top of a thin (nanometer range) ice layer in contact with the substrate. After annealing, a contiguous flat film was formed. Between −20 and −10 °C and at a relative humidity of ~83%, the film consisted of a solid ice layer ~7 Å thick, covered by a liquid-like layer 50±5 Å thick. When the temperature was raised above 0 °C, droplets formed, which subsequently evaporated. Comparison of results obtained in the various AFM operation modes allowed us to conclude the existence of a liquid-like layer on the ice surface.
 [S0021-9606(99)70539-8]

I. INTRODUCTION

The presence of a liquid-like layer (LLL) on the ice surface and its characteristics have been investigated for many decades. Diverse techniques have been employed to study this problem, but there is still ambiguity about a number of properties, in particular, the conditions of existence and the thickness of the LLL as a function of temperature.[1,2] Depending on the experimental conditions and measurement method used, the reported thickness of the LLL varies by as much as a factor of 100 for a given temperature.[1]

Recently, atomic force microscopy (AFM) has been applied to investigate the LLL on the surface of bulk ice crystals.[3–7] The jump-in distance during the approach of the AFM tip to the ice surface was assumed to be indicative of the presence of the LLL and used to probe its thickness. It was found that the upper limit for the thickness of the LLL on bulk polycrystalline ice surfaces varied between 12 nm at −24 °C and 70 nm at −0.7 °C.[7]

Here, we present results of combined noncontact, contact, and lateral force microscopy experiments of very thin (in the nanometer range) ice films grown on mica substrates. Because of their thickness, the properties of these films might be strongly influenced by the substrate and therefore differ substantially from the surface properties of bulk ice. Nevertheless, nanometer-thick (NMT) ice films are likely to coat frosted surfaces of materials in undersaturation conditions, and are therefore relevant to many environmental phenomena. Noncontact microscopy using electrostatic forces, called scanning polarization force microscopy (SPFM), was recently introduced to image liquid films on flat substrates with high lateral (≈50 nm) and vertical (≈0.1 nm) resolution, and is therefore a promising method to probe the LLL on the ice surface.[8] In SPFM, a bias voltage is applied to a conducting tip with respect to the grounded sample holder (the sample does not need to be a conductor). The electric field around the charged tip induces a polarization charge distribution on the sample surface. The resulting long-range electrostatic force is detected at a tip-to-sample distance of several hundred angstroms. Therefore, the tip does not mechanically disturb the surface.

When operated in the contact mode, on the other hand, the liquid phase on the surface cannot be imaged because the tip penetrates it. The comparison of contact mode and SPFM images thus permits us to distinguish between liquid and solid components of the ice surface. The lateral (or frictional) force images help us to identify variations in structure and chemical composition of the surface and reveal, for example, the coverage of a substrate by a solid film (as long as substrate and film have different frictional properties).[9] This combination of AFM operation modes allows us to distinguish ice from water (contact mode vs SPFM images) and ice from mica (lateral force image), as will be shown here.

II. EXPERIMENT

The experiments were performed using a home-built AFM housed in a vacuum chamber. The experimental setup has been described in detail in a previous paper.[10] However, the main features of the apparatus will be summarized briefly.

The sample is mounted on a support connected to a liquid nitrogen reservoir by a copper braid. A resistor is attached to this support for simultaneous heating. The temperature of the sample holder (T_s) can be controlled in a range from −60 to 80 °C using a temperature controller.[11] The accuracy of the temperature adjustment is better than ±0.25 °C. To control the super- or under-saturation of water vapor over the ice layer, a macroscopic ice reservoir is created by condensation on a cooled thermoelectric Peltier element[12] mounted in the chamber. A separate temperature controller maintains the temperature of the reservoir (T_{res}).[11]

a)Electronic mail: salmeron@stm.lbl.gov

The super- or under-saturation of the sample is determined by the ratio of the equilibrium vapor pressures, p_{res} at T_{res} and p_s at T_s.[13] The relative humidity with respect to the sample (RH, in percent) is then $100\times p_{\mathrm{res}}/p_s$. Both T_{res} and T_s are measured using thermistors (3 kΩ@25 °C). The thermistors are calibrated using the equilibrium vapor pressure of water, which condensed either at the reservoir or on the sample.

To prevent excessive condensation of water vapor on the mica substrate, T_s was always kept 2 °C above T_{res} throughout the experiment. This corresponds to RH=80%±5% at −36 °C and RH=83%±4% at −17 °C.[14] Under these conditions, the macroscopic amount of ice at the reservoir maintains a constant vapor pressure p_{res}, which is accurately controlled by T_{res}.

The mica samples were cleaved *in situ* in the bell jar vacuum chamber. Before cleaving, the chamber was evacuated to its base pressure ($\sim 10^{-6}$ torr). Distilled water with a specific resistivity of 18.2 MΩ cm was used as a source of vapor. The water was degassed by several cycles of freeze, pumping, and thawing. During the experiments, the water vapor pressure was in the range of 0.01 to 20 torr, as measured using a capacitance sensor pressure gauge.

The home-built AFM is controlled by a commercial feedback electronic unit.[15] Triangularly shaped silicon cantilevers with a spring constant of 0.4 N/m are used.[16] The cantilevers are boron-doped and have a resistivity of 10^{-3} Ω cm. Typical normal forces in the contact mode experiments are in the range of 10 to 30 nN. The SPFM experiments were performed with a tip-to-sample distance of ~20 nm, and a bias voltage of 10 V applied to the cantilever while the sample holder was kept at ground potential. Due to the good electrical conductivity of the cantilevers, it was not necessary to apply an additional metallic coating to the cantilever. (The backside of the cantilever is, however, gold-coated by the manufacturer for better reflectivity.) The acquisition time for a single image is 2 to 3 min.

The scan direction in the SPFM images was chosen to be parallel to the cantilever axis (left to right, in our images) because in this direction the cantilever was found to be most stable in noncontact imaging. In the contact and lateral force mode experiments, the cantilever was scanned perpendicular to its axis (top to bottom, in our images). Due to the different scan directions in contact mode and SPFM images, a drift of the sample causes different distortions in the images. All images shown here have been corrected for drifts.[17]

Special care has to be taken during AFM experiments to avoid any unwanted influence of the tip on the ice surface, such as heating due to temperature differences between tip and sample, and frictional or pressure melting. In the following, we consider the possible effect of the tip on the ice surface during scanning.

A. Temperature difference between tip and sample

The cantilever can be warmed through the holder to which it is clamped, which is at room temperature. Another source of heating is the impinging laser beam, which is reflected by the cantilever.[18] The power of the incident beam in our experiments was 0.1 mW at λ=632.8 nm. The bending of the cantilever due to temperature changes provides a simple means to determine its temperature. The backside of the silicon cantilever is coated with 5 nm of titanium and 30 nm of gold for better reflectivity.[16] When the tip is brought in the vicinity of a colder surface, its temperature decreases and it bends upwards (away from the sample surface), due to the difference in the linear thermal expansion coefficients of Si (2.5×10^{-6} K^{-1}), Ti (8.6×10^{-6} K^{-1}), and Au (14.2×10^{-6} K^{-1}).[19] With a tip-to-surface distance of 20 nm, the bending of the cantilever as a function of sample temperature was measured to be 200±15 nm/ °C. This is in good agreement with the calculated value of 180±35 nm/ °C, which was computed from the known dimensions of the lever and the thermal expansion coefficients of its components.[20] Through this measurement, we know that the temperature of the cantilever is fairly close to that of the sample surface (within 5 °C), in spite of the heating effect of the laser beam. A beneficial effect of the cantilever being slightly warmer than the sample is that it prevents ice from condensing on the tip.

To ascertain if the tip is damaging the ice due to heating, it was left for 30 min at a fixed position in contact with the surface of the NMT ice film. SPFM images taken before and after the contact showed no differences in the film morphology.

B. Pressure melting

Another possible cause for damage of the ice surface by the tip is pressure melting. At 0 °C the melting point depression due to pressure is -7.37×10^{-8} °C/Pa.[21] Although the normal forces exerted on the surface in the contact and lateral force measurements are weak (nN range), the pressure is high due to the small contact area between tip and sample (nm range). The size of the contact area can be estimated using the Hertz model[22] and the macroscopic elastic constants of Si and ice.[6] For our cantilevers, with a force constant of 0.4 N/m and a normal force of 20 nN, the melting point of ice should decrease by 14 °C for a tip with 100 nm radius, and 21 °C for a tip with radius of 70 nm.[23] (At sample temperatures below −22 °C, pressure melting does not occur. Instead, phase transitions to high-pressure forms of ice could be expected if the force exerted by the tip is sufficiently large.[23]) The exact value of the contact area, however, is not known in the experiment, and the effect of pressure melting is therefore difficult to predict. To assess the effect of load, we imaged the surface in contact mode with loads up to 150 nN, which is well above the values applied during the acquisition of contact mode images in this paper. No changes in the height of the NMT ice film were observed as compared to images acquired in the low-load regime. We will therefore assume that the heights measured in the contact images taken in the low-load regime (as in the data presented here) represent the true heights of the solid part of the ice layer.

C. Frictional heating

It has been shown in a number of experiments that the frictional heat produced by the relative motion of a slider on

the surface can be large enough to melt ice.[24,25] We can estimate the influence of this effect by comparing the energy required to melt a certain volume of ice (Q_m), the energy generated by friction (Q_f), and the energy conducted away into the ice or mica substrate and tip (Q_c) during the contact. If $Q_m < Q_f - Q_c$, then melting will take place. For the computation of Q_m, Q_f, and Q_c, we follow the method presented in Ref. 26. The heat required to melt a bilayer of ice of 10 nm diameter (i.e., in the contact zone) is $Q_m \approx 5 \times 10^{-18}$ J. Assuming typical values for the scan speed (10^{-5} m s^{-1}), tip radius (50 nm), lateral force (30 nN), load (20 nN), and corresponding Hertzian contact radius (10 nm), a sample temperature of $-20\,^{\circ}$C and a tip temperature of $-15\,^{\circ}$C, we get $Q_f \approx 3 \times 10^{-16}$ J and $Q_c \approx 7 \times 10^{-14}$ J. This means that, although the frictional heat would be sufficient to melt several ice bilayers, the high thermal conductivity removes this energy very efficiently into the bulk of the tip and the mica substrate. Therefore, under our experimental conditions, frictional heating should not melt the NMT ice film.

III. RESULTS

All the data presented in this paper were collected in a single experiment. At the beginning of the experiment, the chamber was evacuated to its base pressure of 10^{-6} torr. Then, water vapor was introduced until a pressure of 4.4 torr was reached (corresponding to a relative humidity of 24% at the ambient temperature of 21 °C). The mica sample was cleaved in the presence of this water vapor.[27] The SPFM contact and lateral force images acquired subsequently indicated that the surface was atomically flat without any cleavage steps over tens of micrometers. The contrast in the SPFM, as well as in the lateral force images, showed no variations, indicating that the freshly cleaved surface was free of contamination and possessed a homogeneous chemical composition.

The sample and the reservoir were then cooled to $T_s = -36\,^{\circ}$C and $T_{res} = -38\,^{\circ}$C, respectively, in the presence of the vapor. Ice condensation on the reservoir could be seen by the naked eye. The equilibrium water vapor pressure was 0.11 torr, corresponding to RH=80%. SPFM images taken throughout the cooling process under these conditions showed no change in the surface contrast.

The sample temperature was then decreased to $-45\,^{\circ}$C for about 20 s. This caused the mica surface to be supersaturated with respect to the water vapor pressure. Afterwards, T_s was increased back to $-36\,^{\circ}$C. T_{res} was kept constant during this time. Figure 1(a) shows an SPFM image taken after this temperature digression. The surface is covered with droplets, which have a maximum height of 12 nm and a maximum diameter of 2 μm at the base. Figure 1(b) shows a topographical image acquired in contact mode at the same location just after acquisition of the SPFM image. T_s and T_{res} are the same as in Fig. 1(a). Two types of features can be distinguished: (a) large, nearly round, flat platelets 0.2 to 0.3 nm high relative to the substrate, and (b) small particles with a height of 2 nm situated preferentially at the rim of the platelets (seen as bright features in the image). The nature of these particles is still unclear. They were found to occur in many cooling experiments on mica. After warming the sample to room temperature, the bright particles (hereafter, we shall use this name for simplicity) could still be observed. The solid platelets of NMT ice and the droplets above them grow outside the areas occupied by the particles, whose shape and size do not change during the course of the experiment.

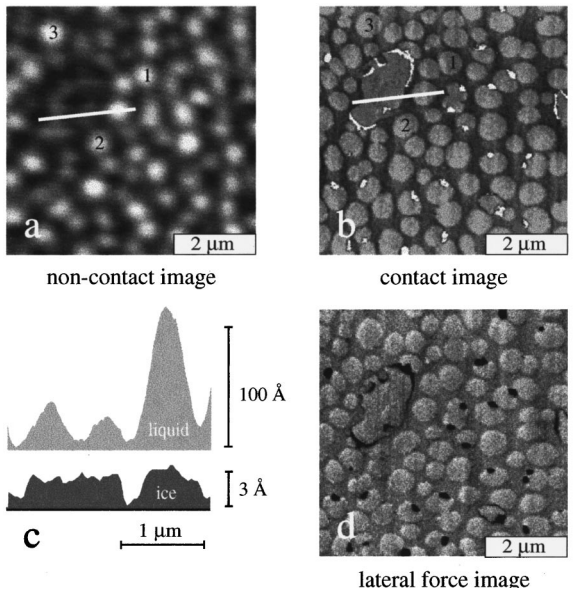

FIG. 1. (a) SPFM image showing liquid droplets on a mica substrate at $T_s = -36\,^{\circ}$C and 20% undersaturation (80% relative humidity). They were formed after exposing the mica to supersaturated water vapor at $-45\,^{\circ}$C for a few seconds. The maximum height of the droplets is 12 nm, and the maximum diameter at their base is 2 μm. (b) Contact mode image acquired at the same location as (a) after the SPFM image was taken. Large, nearly round ice platelets with a height of 0.2 to 0.3 nm relative to the substrate (i.e., one bilayer thick) can be seen. The platelets are at the same location as the droplets shown in (a). The bright spots in the image are 2 nm high and are probably due to contamination. The numbers given in (a) and (b) mark corresponding sample spots in the SPFM and contact mode images, respectively. (c) Comparison of cross sections taken along the line indicated in (a) and (b). All droplets are sitting on ice platelets. (d) Lateral force image taken simultaneously with the contact mode image. A brighter contrast means a higher lateral force. The lateral force is highest on the platelets, and lowest on the bright particles.

Cross sections along equivalent lines in Figs. 1(a) and 1(b), as shown in Fig. 1(c) clearly indicate that the position of the round NMT ice platelets coincides with that of the droplets imaged using noncontact SPFM. Although the size of the drop appears to fill or even exceed the size of the ice platelets, this is an effect of the lower lateral resolution in the SPFM imaging mode. In fact, the droplets are smaller than the platelets and form a finite contact angle of $3.0^{\circ} \pm 0.5^{\circ}$. This can be best observed in the case of the large platelet in Fig. 1 [because of contrast, it is best seen in the contact image of Fig. 1(b)]. Several small drops cover this platelet. We have observed in other experiments (which are not shown in this paper), under identical thermodynamic conditions, a continuous ice film instead of platelets, and similar droplets with identical contact angles on top of this film. These results demonstrate that the liquid on the surface of the solid phase possesses a nonzero contact angle under these conditions.

A lateral force image acquired simultaneously with the

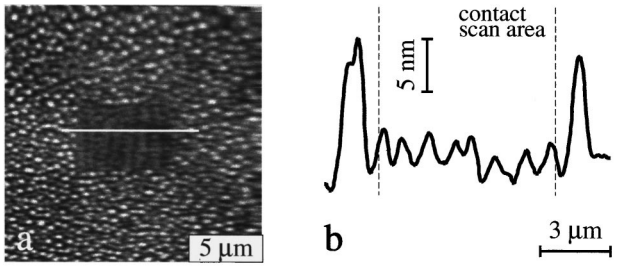

FIG. 2. (a) SPFM image taken after the contact mode image of Fig. 1(b) under identical pressure and temperature conditions. The scan range was increased compared to the images shown in Fig. 1. The morphology of the regions within and outside the contact scan area differs, showing that material was removed during the contact scan. (b) Cross section taken along the line indicated in (a). The maximum height of the droplets outside the contact scan area is 12 nm, i.e., the same as in Fig. 1(a). Inside the contact scan area, the height is reduced to $\leqslant 5$ nm.

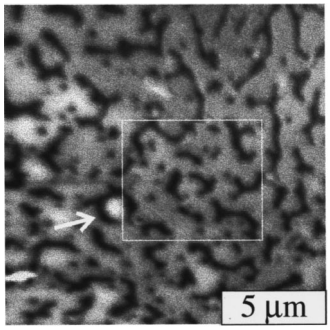

FIG. 3. (a) SPFM image acquired after the sample temperature T_s was increased to $-17\,^{\circ}\mathrm{C}$. The sample location is different from that of Figs. 1 and 2. A contiguous liquid film with an average height of 5.5 nm has replaced the droplets. A few droplets, disconnected from the rest of the film, can still be observed in some places, as shown by the arrow.

contact topography is presented in Fig. 1(d). A brighter contrast means a higher lateral force. The tip experiences the highest lateral force on the ice platelets, and the lowest on the bright particles. The increased lateral force on the ice platelets as compared to the surrounding substrate could be partly due to an increased adhesive force in the liquid film. This effect is small, however, since the large island not completely covered by liquid does not show any detectable lateral force contrast due to the incomplete coverage by the liquid. The ratio of the lateral force measured on the NMT ice platelets in comparison to the substrate is similar to the results obtained in our previous investigations of ice dendrites grown on mica,[10] and provides further evidence that the flat platelets are indeed ice.

After scanning the surface in contact mode, the scan range was increased and a new SPFM image was acquired [Fig. 2(a)]. The temperature of the sample and the reservoir are the same as in Fig. 1. The SPFM image shows that the droplets in the previous contact scan area have been mostly removed. Some residual material seems to be arranged along the contact scan direction (vertical). A cross section along the line indicated in Fig. 2(a) is shown in Fig. 2(b). Inside the area previously scanned in contact, the corrugation is below 5 nm. Outside of it, however, droplets with the same height distribution as in Fig. 1(a) are observed. This experiment indicates that the morphology of the film outside the contact scan area has not changed within the 30 min that elapsed between acquisition of Fig. 1(a) and Fig. 2(a).

The sample was then annealed by increasing its temperature to $-17\,^{\circ}\mathrm{C}$, while at the same time increasing the reservoir temperature to $-19\,^{\circ}\mathrm{C}$. The water vapor pressure in equilibrium with the reservoir at $T_{\mathrm{res}}=-19\,^{\circ}\mathrm{C}$ was 0.84 torr, i.e., RH=83%. As shown in the SPFM image of Fig. 3 (acquired at a location different from that in Figs. 1 and 2), annealing produced a smooth film. The substrate is now almost completely covered by a flat percolating film with a height of 5.5 ± 0.5 nm. In some places, a few residual droplets can still be observed.

After the SPFM scan, a contact image was acquired at the location indicated by the square in Fig. 3. The topography obtained [see Fig. 4(a)] is similar to that of the SPFM image. The small bright particles appear again with about the same density and height as in Fig. 1(b). The edges of the contiguous film are apparently pinned to these particles. The height of the film obtained from the contact image is now 0.7 to 0.8 nm, i.e., about twice as thick as before. The images of the film remained unaltered during contact mode imaging, as proven by acquiring several consecutive images of the same area. The different heights measured in noncontact and contact modes (5.5 vs 0.7 nm) indicate the presence of a soft, liquid-like film on top of a stiff, solid substrate (the NMT ice film).

The lateral force image of the same area is shown in Fig. 4(b). As in Fig. 1(d) there are three different contrast levels in the image. The lateral force is highest on the surface of the NMT ice film and lowest on the particles. Since the images in Figs. 1(d) and 4(b) were taken using the same cantilever and the same normal force (20 nN), the lateral force values can be compared. The ratio of this force on the NMT ice, substrate, and particles is found to be the same in both Figs. 1(d) and 4(b). This indicates that the NMT ice film under the droplets in Fig. 1(d) has the same frictional properties as the film in Fig. 4(b).

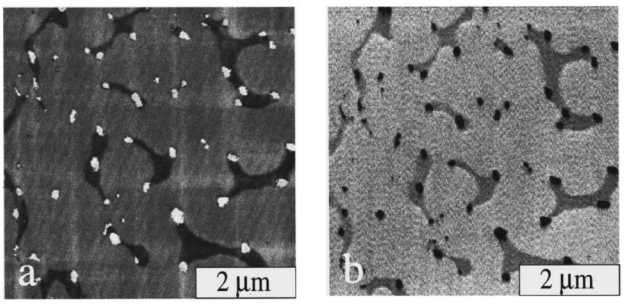

FIG. 4. (a) Contact topographic image acquired at the location indicated by the square in Fig. 3. The height of the ice film is 0.7 to 0.8 nm, corresponding to two bilayers. The bright particles show about the same density and height as in Fig. 1(b). The edges of the ice film are apparently pinned to these particles. (b) Lateral force image taken simultaneously with the contact scan shown in (a). The ratio of the friction contrast of platelets/substrate/particles in Fig. 1(d) is equal to the ratio of the corresponding values of film/substrate/particles in Fig. 4(b). This indicates that the ice layer at the bottom of the droplets in Fig. 1(d) has the same frictional properties as that in (b).

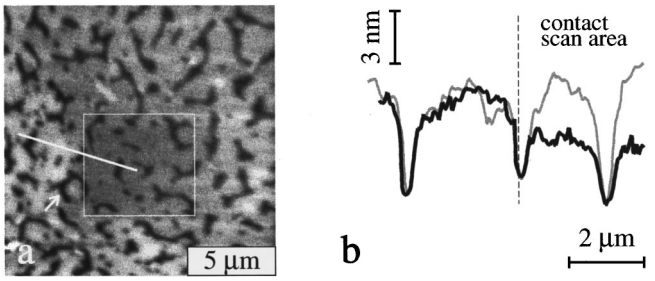

FIG. 5. (a) SPFM image taken at about the same location as in Fig. 3 under identical pressure and temperature conditions. The previously scanned contact area is indicated by a square. (b) Cross section along the line indicated in (a) (black line). The film in the contact scan area is 3.0 ± 0.5 nm thinner than the rest of the film. For comparison, a cross section taken in Fig. 3 (i.e., before contact) at exactly the same position is also shown (gray line). Comparison of both cross sections shows that material was removed during contact scanning.

Figure 5(a) shows a larger SPFM image acquired at about the same location as in Fig. 3 (T_s and T_{res} are still the same as in Figs. 3 and 4). The area previously scanned in contact mode is indicated by a square. The shape of the film has not changed in the contact scan area [unlike the case of Figs. 1(b) and 2(a)]. However, a cross section shows that the film in the contact scan area is 3.0 ± 0.5 nm thinner than the rest of the film [see the black line in Fig. 5(b)]. A cross section taken in Fig. 3 (i.e., before the contact scan) at exactly the same position is also given [the gray line in Fig. 5(b)]. Comparison of both cross sections shows that material has been removed from the film during contact scanning.

Figure 6(a) shows an SPFM image of the surface after warming the sample and reservoir to $T_s=-4\,^{\circ}\mathrm{C}$ and $T_{\mathrm{res}}=-6\,^{\circ}\mathrm{C}$, respectively. The water vapor pressure is now 2.59 torr. The images correspond to the surface area located at the bottom of Fig. 5(a). As can be seen, the main morphological features are similar in both figures (the arrows mark two corresponding features in each figure). This is perhaps not surprising since the relative humidity at this pressure is 79%, only slightly lower than in Fig. 5(a) (83%). However, a closer look reveals that some holes have changed their shape, presumably due to a higher mobility of the water molecules at the elevated temperature [see the holes marked by arrows in Figs. 5(a) and 6(a)]. In addition, the film height is reduced to 4 nm in the areas that have not been scanned in contact before. Figure 6(b) shows an image taken after warming the sample to $0\,^{\circ}\mathrm{C}$ ($T_{\mathrm{res}}=-2\,^{\circ}\mathrm{C}$, $p_{\mathrm{res}}=2.86$ torr, RH=63%). Due to the lower relative humidity, the evaporation of the film is now clearly visible and manifests itself in a widening of the holes in the film and a decrease in thickness to 3 nm.

Figure 6(c) shows an image of the surface after the sample has been warmed to $5\,^{\circ}\mathrm{C}$. The vapor pressure in the chamber is 2.80 torr, which corresponds to RH=43%. The fraction of the substrate surface covered by the film is less than 50%, and its morphology is now similar to that of a water film on mica previously observed at room temperature.[8] The height of the film as measured in SPFM is the same as in Fig. 6(b) (3 nm). Further warming of the sample to $10\,^{\circ}\mathrm{C}$ caused the film to collapse into droplets with a maximum height of 7 nm [see Fig. 6(d)]. The droplets evaporate over a period of about 30 min while the substrate is allowed to warm up to room temperature (the background pressure was kept at 2.8 torr). Contact mode images taken after the evaporation show a weak lateral force contrast at the former positions of the droplets. The contrast vanishes after the relative humidity in the chamber is increased to a value of about 40% and is attributed to the rearrangement of ions on the mica surface.[7]

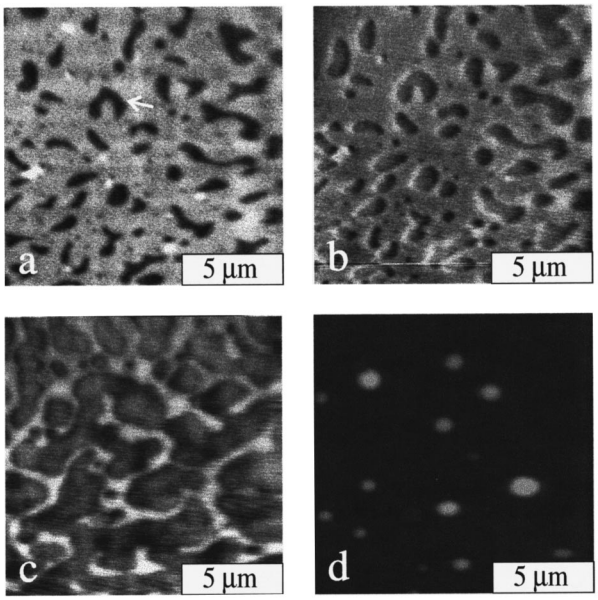

FIG. 6. SPFM images from the same area as in Fig. 5 (compare features marked by the arrow), acquired during warming of the sample and reservoir at: (a) $T_s=-4\,^{\circ}\mathrm{C}$, $p_{\mathrm{H_2O}}=2.59$ torr, (b) $T_s=0\,^{\circ}\mathrm{C}$, $p_{\mathrm{H_2O}}=2.86$ torr, (c) $T_s=5\,^{\circ}\mathrm{C}$, $p_{\mathrm{H_2O}}=2.80$ torr, and (d) $T_s=10\,^{\circ}\mathrm{C}$, $p_{\mathrm{H_2O}}=2.76$ torr. The reservoir was always $2\,^{\circ}\mathrm{C}$ colder than the sample. Increased mobility of the water molecules close to the melting point manifests itself as a change of the morphology of the holes [compare the holes marked by arrows in Figs. 5(a) and 6(a)]. The film thickness decreased to $\approx$4 nm at $T_s=-4\,^{\circ}\mathrm{C}$, and further to 3 nm at $T_s=0$ and $5\,^{\circ}\mathrm{C}$. Eventually, the flat film collapses into droplets, which then evaporate [see Fig. 6(d)].

IV. DISCUSSION

A. Contact and noncontact thickness measurements

We begin the discussion by considering the principal differences between the height measurement in contact mode and SPFM imaging. In contact mode, the tip traces the surface along lines of constant repulsive force. Deviations from the true topography can occur due to plastic or elastic deformation of the surface. In the present case, we must consider pressure-melting and frictional-melting effects as well. As shown in the experiment chapter, neither phenomenon appears to affect the heights of the NMT ice film under the conditions of our experiments.

In SPFM imaging, the tip traces lines of constant attractive force. The SPFM image is generated by superposing three contributions: the topography of the solid part of the surface (visible also in contact mode), the liquid part of the surface (not visible in contact mode), and electrostatic contributions. The latter ones can be caused by contact potential differences (e.g., variations of the surface charge distribution), and by differences in local dielectric properties (including contributions of ion mobility).

We know from the similarity of SPFM images acquired at both+and−bias that the contribution from contact potential differences is minimal. We can estimate the contribution of dielectric constant (ε) variations to the measured height by noting that ε enters the electrostatic force through the ratio $(\varepsilon-1)/(\varepsilon+1)$. If we use $\varepsilon=7$ (mica) and $\varepsilon=80$ (water/ice), the difference in topography could be on the order of 25%. In fact, it should be much smaller than that because, at dc and low frequencies, $\varepsilon\rightarrow\infty$, due to the presence of mobile ions. In other words, the SPFM topographic heights should be close to the real heights. The large difference observed between the heights in contact and noncontact images therefore indicates that there is a soft or liquid-like film over the flat NMT ice film.

B. Nucleation and growth of thin ice

After the sample was cleaved at room temperature at a relative humidity of 24%, nuclei of an ice-like bilayer should be covering the mica, as shown in recent sum frequency generation (SFG) experiments[28] and theoretical studies.[29] At room temperature, this bilayer saturates at about 80% relative humidity. In addition, it is epitaxial with the mica and under tension (lattice mismatch with the mica is 10%). A very important property of this bilayer is that it contains no free OH groups, i.e., all the H atoms are tied into H bridges to other molecules or to the surface.[29] In the room-temperature SFG study,[26] multilayer growth of water above the first bilayer was only observed after increasing the humidity to 90%. This indicates an increase in the film energy when the thickness is larger than the bilayer due to accumulation of strain (from mismatch) and electrostatic energy terms (from dipole orientation).

We believe that the same arguments apply in the present experiments. Condensation on top of the first ice bilayer occurred only after strong supersaturation conditions were established by cooling to $-45\,^{\circ}\mathrm{C}$. Under these conditions, ice platelets covered by liquid droplets form [Fig. 1(a)].

The incomplete coverage of the substrate by the ice/water film could be due to: (1) contamination of the mica substrate, which prevents the film from spreading; (2) the growth conditions, i.e., high supersaturation, leading to a number of nucleation sites distributed over the surface which have not had enough time to grow and interconnect in the short period of supersaturation (only a few seconds); or (3) nonequilibrium phenomena, such as that observed earlier by Elbaum and Lipson.[30] It is difficult to determine which of these possibilities is causing the patchy (platelets) structure of the ice/water film, but we believe that contamination is the most likely one. We have, as mentioned above, observed in other experiments a continuous film under the same thermodynamic conditions as in the experiments described in this paper. This means that nonequilibrium phenomena are probably not responsible for the shape of the islands. The variability observed in the structure of this first ice layer, i.e., sometimes forming a continuous film and sometimes platelets (as in the figures presented here), supports the idea of contamination.

The existence of supercooled water droplets at a temperature of $-36\,^{\circ}\mathrm{C}$ (as shown in Fig. 1) is not surprising. It has been demonstrated that the onset temperature of crystallization depends critically on the volume of the droplets.[31] The smaller the droplets, the less likely the presence of an impurity, i.e., a nucleation center. The droplet volumes in our case are small ($\leqslant 0.2\ \mu\mathrm{m}^3$), compared to the critical droplet size for heterogeneous nucleation expected at $-36\,^{\circ}\mathrm{C}$ mentioned in Ref. 31 ($\approx 500\ \mu\mathrm{m}^3$).[32] It can therefore be expected that supercooled droplets will form during condensation of water on mica. It is interesting to note that, under these conditions, the liquid does not spread on the ice completely. The contact angle of the droplets estimated from their height and base diameter is $3.0^{\circ}\pm 0.5^{\circ}$.

The contact mode scans [Fig. 1(b)] indicate that the thickness of the NMT ice platelets under the droplets is 0.2–0.3 nm. At the given substrate temperature and background pressure, ice *Ih* is expected to grow on the mica surface. Ice *Ih* possesses hexagonal symmetry with lattice constants of $a=0.451$ nm and $c=0.735$ nm (at $-35\,^{\circ}\mathrm{C}$).[33] Relative to the {0001} plane, a thickness of 0.2–0.3 nm would correspond to just one ice bilayer (as defined in Ref. 34). It is the peculiar nature of this ice bilayer, which is highly stressed and exposes no free OH bonds, that is at the origin of the relatively large contact angle measured. The transition from flat layers to droplets is likely a result of the relaxation of stress, as in Stranski–Krastanov mode growth, with the difference that here the 3D growth is liquid rather than solid.

Water droplets on top of the ice surface have also been observed in earlier experiments at the triple point.[35–37] It was demonstrated that, in the presence of pure water vapor (i.e., under gas phase conditions comparable to those in our experiments), neither the {10–10} nor the {0001} face show complete wetting by a water film.[35] However, introduction of air into the chamber caused the droplets to spread, a behavior that was explained as due to the introduction of impurities, which reduce the free energy of the solid–liquid and/or liquid–vapor interface and thus promote spreading.[35] In a theoretical work, the contact angle of supercooled water was calculated to be $\sim 0.2^{\circ}$.[38] All these results were achieved, however, for the case of a thick ice surface in equilibrium with its vapor and at (or close to, in case of Ref. 38) the triple point. The droplets found in our experiments are formed on the NMT ice film at RH$\approx$80% and at temperatures far away from the triple point. Therefore, comparison with the results presented in Refs. 35–38 might not be legitimate.

The noncontact image acquired after Fig. 1 (Fig. 2) shows that there has been a substantial loss of material in the contact area due to the influence of the tip. Since we did not observe accumulation of material at the rim of the contact area, we can assume that the water has evaporated, probably due to the slightly higher temperature of the tip with respect to the sample surface. The height of the features obtained from the SPFM image in the modified area (2–3 nm), however, is still ten times higher than that measured in contact mode (0.2–0.3 nm). This indicates that a liquid layer on top of the ice still exists.

C. Annealed ice–water film

A flat contiguous film is formed after annealing the sample to $-17\,^{\circ}\mathrm{C}$, while maintaining the same relative hu-

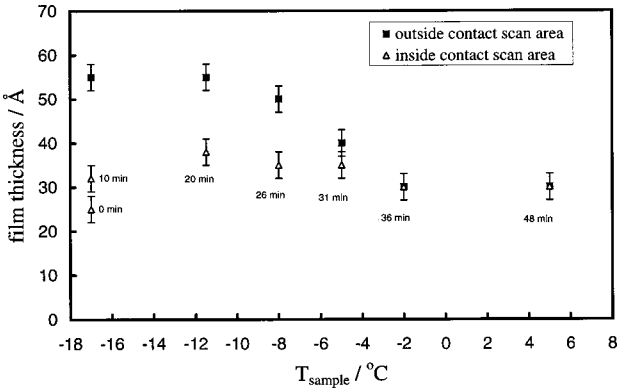

FIG. 7. Comparison of the thickness of the film within and outside the area modified by contact scanning in Fig. 4(a). The thickness was 5.5 nm in both areas before the contact scan. This value remained unaltered outside the contact scan region (■), but is reduced to 2.5 nm inside the contact scan area (△). The first SPFM image acquired after the contact scan was taken at time 0 min. When the surface is measured again 10 min later under identical experimental conditions, the height of the film outside the contact scan area is still 5.5 nm, while it has increased to 3.2 nm within the contact scan area, i.e., the surface is ''healing.'' Above −10 °C the relative humidity decreased below 80%, which resulted in a loss of height to about 3 nm. At temperatures close to the melting point, the heights within and outside the contact scan area are equal.

midity of 80%. The difference in heights measured in contact mode [0.7–0.8 nm, Fig. 4(a)] and noncontact SPFM mode (5.5 nm, Fig. 3) indicates that a liquid film (~4.8 nm thick) is present on top of the NMT ice layer. The ice thickness has increased to two bilayers, indicating that some of the liquid has solidified.[39] The important observation is that the liquid is now spread on the NMT ice film and appears flat. At first, one might think that this is an indication that the droplets are a metastable form, perhaps due to the limited size of the platelets. However, we have observed in other ice growth experiments on mica that the transition from the droplet-shaped structures observed at −36 °C [cf. Fig. 1(a)] to the flat contiguous film observed at −17 °C (cf. Fig. 3) is reversible in both directions.[40] Therefore, these types of morphology correspond to the equilibrium state of water on the NMT ice films.

In Fig. 7, we compare film thickness within and outside the contact scan area of Fig. 4(a) measured in the SPFM mode. Before the contact scan, the film thickness was 5.5 nm in both areas [see traces in Fig. 5(b)]. This value remained unaltered in the unperturbed region, but is reduced to 2.5 nm after a contact scan. When the perturbed part of the surface is measured again 10 min later, the height of the film in the undisturbed area is still 5.5 nm, while it has increased to 3.2 nm within the area previously scanned in contact. This height increase is homogeneous over the entire area, indicating that the film grows by water adsorption from the gas phase rather than from liquid flowing in from the surrounding area. During warming of the sample, the height of the film remains virtually constant, until the temperature increases to above −10 °C. This is the point where the relative humidity starts to decrease below ~80%. At temperatures close to the melting point, the heights within and outside the contact scan area become equal (cf. Fig. 7). A similar effect was observed for adsorption isotherms of water on gold substrates, which were acquired at room temperature using a quartz crystal microbalance.[41] The water layer thickness depended only on the relative humidity.

From the data in Fig. 7, we can determine the thickness of the LLL on the NMT ice on mica. This is the difference between the heights measured using SPFM (before the contact scan) and in contact mode. In the present case (Figs. 3 and 4), the LLL thickness is 5.5 nm − 0.7 nm = 4.8 nm at −17 °C.

The results presented in the previous section demonstrate that water, which is condensed on mica at sufficiently low temperature, forms a solid layer a few ice bilayers thick, covered by a liquid phase. Although the comparison is not necessarily valid, it is instructive to consider the topic of surface melting, which has been observed experimentally for bulk ice crystals.[1,2] Recent x-ray diffraction studies[42] could verify a theoretical model by Fletcher[43] for the formation of an LLL on the ice surface. The theory is based on the existence of a positively charged surface layer on ice, due to the orientational ordering of H_2O dipoles at the surface. Sliding electrification experiments confirmed that the surface of ice is positively charged.[44] To compensate for the surface charges, a mesoscopic screening layer that is highly disordered (Bjerrum defects) is present in the subsurface region.[43] The loss of long-range order within this transition layer leads to a liquid-like structure at the ice surface. In the aforementioned x-ray diffraction studies, the thickness of the transition layer was found to be greater than 25 nm in the temperature range from −10 to −20 °C on the (10–10) face.[42,45] Fletcher's model[43] could perhaps be used to explain our data, but in the opposite direction. The ordered, dipole-oriented layer of ice might force the growth of a transition liquid-like layer on top of it. In addition, the highly strained form of our NMT ice film would further promote the formation of an LLL, where the strain is relieved. Further experiments to determine the loss of dipolar orientation as a function of thickness, such as sum frequency generation (see Ref. 28) and others, are currently being prepared in our laboratory.

There are other effects that should also be considered in our case. One is the influence of the potassium ions on the mica surface. Recent SPFM studies of water adsorption on mica at room temperature have shown that, at a relative humidity above 20%, some of the potassium ions become mobile.[46] During growth of the ice film, K^+ ions will stay either at the mica/ice interface or, if hydrated, could move to the free ice surface. This would imply that the liquid layer observed on the ice surface might not consist of pure water, but rather of a KOH solution with a certain concentration, depending on the amount of K^+ ions in the solution. One can put a limit to the fraction of solvated ions from the density of the K^+ at the mica surface (2×10^{18} m^{-2}) and water molecules in a bilayer (10^{19} m^{-2}). At a water film thickness of 5.5 nm (as in Figs. 3 to 5), there would be a 1 M solution of KOH on the surface in the extreme (and unlikely) case in which all the surface K ions were fully solvated (i.e., dissolved). This would lower the *bulk* freezing point of water by 2.4 °C[19] and can therefore not account for the observation of a liquid layer on the ice surface at −17 °C. On the other hand, a small fraction of impurities (smaller than necessary

for bulk freezing point depression) can affect the thickness and existence of an LLL on the ice surface significantly, as shown in a recent theoretical work by Wettlaufer.[47] However, ice growth experiments on ion-free substrates (such as silicon) show the existence of a liquid water layer at temperatures down to −40 °C and therefore prove that the liquid layer on the ice film grown on mica substrates is not caused by melting point depression due to dissolved ions.[48]

V. SUMMARY

Combined AFM investigations performed in noncontact (SPFM), contact, and lateral force imaging modes have shown that nanometer-thin (NMT) films of ice grown on mica substrates at temperatures below −30 °C are in contact with supercooled liquid droplets. These droplets do not cover the ice film completely and form a contact angle of 3.0 ±0.5°. Annealing to ~−17 °C leads to the thickening of the solid part of the NMT ice film and to spreading of the liquid layer on its surface. The solid NMT ice film can support the pressure exerted by the tip in contact. Contact, however, removes part of the liquid layer film, even at the lowest loads. The loss of liquid did not recover completely until the temperature increased to above −10 °C, indicating a high viscosity of the liquid-like layer.

ACKNOWLEDGMENTS

This work was supported by a Laboratory Directed Research and Development grant from the Lawrence Berkeley National Laboratory through the Director, Office of Science, Office of Basic Energy Sciences, Materials Science Division of the U.S. Department of Energy under Contract No. DE-AC03-76SF00098. The authors thank L. Xu, F. Rieutord, T. Inoue, U. Jonas, and D. F. Ogletree for helpful discussions. H. Bluhm acknowledges support from the Alexander von Humboldt Foundation, Bonn, Germany.

[1] For a review, see V. F. Petrenko, *The Surface of Ice*, U.S. Army CRREL Special Report No. 94-22 (U.S. Army Cold Regions Research and Engineering Laboratory, Hanover, New Hampshire, 1994), and also Ref. 2.
[2] J. G. Dash, H. Fu, and J. S. Wettlaufer, Rep. Prog. Phys. **58**, 115 (1995).
[3] O. Nickolayev and V. F. Petrenko, in *Evolution of Thin Film and Surface Structure and Morphology, MRS Symposia Proceedings, Vol. 355*, edited by B. G. Demczyk (Materials Research Society, Pittsburgh, 1995), p. 221.
[4] C. R. Slaughterbeck, E. W. Kukes, B. Pittenger, D. J. Cook, P. C. Williams, V. L. Eden, and S. C. Fain, J. Vac. Sci. Technol. A **14**, 1213 (1996).
[5] V. F. Petrenko, J. Phys. Chem. B **101**, 6276 (1997).
[6] B. Pittenger, D. J. Cook, C. R. Slaughterbeck, and S. C. Fain, J. Vac. Sci. Technol. A **16**, 1832 (1998).
[7] A. Doeppenschmidt, M. Kappl, and H.-J. Butt, J. Phys. Chem. B **102**, 7813 (1998).
[8] J. Hu, X.-D. Xiao, and M. Salmeron, Appl. Phys. Lett. **67**, 476 (1995); J. Hu, X.-D. Xiao, D. F. Ogletree, and M. Salmeron, Science **268**, 277 (1995).
[9] For a review of lateral force microscopy, see, for example, R. W. Carpick and M. Salmeron, Chem. Rev. **97**, 1163 (1997).
[10] H. Bluhm, S. H. Pan, L. Xu, T. Inoue, D. F. Ogletree, and M. Salmeron, Rev. Sci. Instrum. **69**, 1781 (1998).
[11] Model 325 temperature controller, Newport Corporation, Irvine, California.
[12] Model CP0.8-127-06L, Melcor Corporation, Trenton, New Jersey.
[13] G. W. Bryant, J. Hallett, and B. J. Mason, J. Phys. Chem. Solids **12**, 189 (1959).
[14] The error in the calculation of the relative humidity is caused by the error in the temperature measurement.
[15] STM 100, RHK Technology, Rochester Hills, Michigan.
[16] Ultralevers, Park Scientific Instruments, Sunnyvale, California.
[17] The drift was calculated from the lateral shift of characteristic features of the sample surface in consecutive images.
[18] M. Allegrini, C. Ascoli, P. Baschieri, F. Dinelli, C. Frediani, A. Lio, and T. Mariani, Ultramicroscopy **42–44**, 371 (1992).
[19] *CRC Handbook of Chemistry and Physics*, edited by D. R. Lide, 78th ed. (CRC Press, Boca Raton, 1997).
[20] The error in the calculated value for the lever bending due to temperature changes was computed assuming a ±10% uncertainty in the length of the cantilever, its total thickness, and the thickness of the gold coating. The error in the experimental determination of the cantilever deflection caused by temperature changes is due to the error in the temperature measurement (±0.25 °C) and the uncertainty in the piezo calibration (±0.1 nm).
[21] P. V. Hobbs, *Ice Physics* (Clarendon, Oxford, 1974).
[22] H. Hertz, J. Reine Angew. Math. **92**, 156 (1881).
[23] W. Wagner, A. Saul, and A. Pruss, J. Phys. Chem. Ref. Data **23**, 515 (1994).
[24] F. P. Bowden and T. P. Hughes, Proc. R. Soc. London, Ser. A **172**, 280 (1939).
[25] D. C. B. Evans, J. F. Nye, and K. J. Cheeseman, Proc. R. Soc. London, Ser. A **347**, 493 (1976).
[26] P. Oksanen and J. Keinonen, Wear **78**, 315 (1982).
[27] It is favorable to cleave the mica in the presence of water vapor to avoid charging of the mica sample, and to protect the mica surface from contaminants.
[28] P. B. Miranda, L. Xu, Y. R. Shen, and M. Salmeron, Phys. Rev. Lett. **81**, 5876 (1998).
[29] M. Odelius, M. Bernasconi, and M. Parrinello, Phys. Rev. Lett. **78**, 2855 (1997).
[30] M. Elbaum and S. G. Lipson, Phys. Rev. Lett. **72**, 3562 (1994); S. G. Lipson, Phys. Scr. **T76**, 63 (1996).
[31] C. A. Angell, Annu. Rev. Phys. Chem. **34**, 593 (1983).
[32] Since there are no experimental results for heterogeneous nucleation of ice from supercooled water at −36 °C, we have extrapolated curve no. 1 in Fig. 1 of Ref. 31 to obtain the value for the critical droplet diameter.
[33] N. H. Fletcher, *The Chemical Physics of Ice* (Cambridge University Press, London, 1970), p. 27.
[34] N. Materer, U. Starke, A. Barbieri, M. A. Van Hove, G. A. Somorjai, G.-J. Kroes, and C. Minot, Surf. Sci. **381**, 190 (1997).
[35] M. Elbaum, S. G. Lipson, and J. G. Dash, J. Cryst. Growth **129**, 491 (1993).
[36] W. M. Ketcham and P. V. Hobbs, Philos. Mag. **19**, 1161 (1969).
[37] C. A. Knight, Philos. Mag. **23**, 153 (1971).
[38] M. Elbaum and M. Schick, Phys. Rev. Lett. **66**, 1713 (1991).
[39] The thickness of the ice layer found at −17 °C is independent of the deposition time for deposition times between a few seconds and half a minute. The influence of deposition times longer than half a minute is currently under investigation.
[40] These experiments were performed in the same way as the experiments described in this paper, except that the process was repeated by twice cycling the temperature between −36 and −17 °C. In these experiments, we found the same droplet heights (or film heights, respectively) at the respective temperatures as in the experiments presented here.
[41] J. Krim, E. T. Watts, and J. Digel, J. Vac. Sci. Technol. A **8**, 3417 (1990).
[42] H. Dosch, A. Lied, and J. Bilgram, Surf. Sci. **366**, 43 (1996); **327**, 145 (1995); A. Lied, H. Dosch, and J. H. Bilgram, Phys. Rev. Lett. **72**, 3554 (1994).
[43] N. H. Fletcher, Philos. Mag. **18**, 1287 (1968); N. H. Fletcher, Philos. Mag. B **66**, 109 (1992).
[44] V. F. Petrenko, J. Appl. Phys. **76**, 1216 (1994); V. F. Petrenko and S. C. Colbeck, *ibid.* **77**, 4518 (1995).
[45] The transition layer is situated between the bulk (ordered) ice crystal and the liquid-like layer on the ice surface. The x-ray diffraction studies cited in Ref. 42 could clearly distinguish between the transition layer and a liquid layer at the ice surface that was observed at temperatures higher than −12.8 °C.
[46] L. Xu, A. Lio, J. Hu, D. F. Ogletree, and M. Salmeron, J. Phys. Chem. B **102**, 540 (1998).
[47] J. S. Wettlaufer, Phys. Rev. Lett. **82**, 2516 (1999).
[48] H. Bluhm and M. Salmeron (unpublished).